Front. Phys. China, 2010, 5(4): 393–404
DOI 10.1007/s11467-010-0136-1

REVIEW ARTICLE

Tailoring interacting magnetic nanodots via dimensionality variation of mediating electrons

Li-feng YIN[1], **Jian SHEN**[1,2,†]

[1] *Department of Physics, Fudan University, Shanghai 200433, China*
[2] *Department of Physics and Astronomy, The University of Tennessee, Knoxville, TN 37966, USA*
E-mail: †*shenj5494@fudan.edu.cn*

Received June 29, 2010; accepted July 26, 2010

Nature produces ferromagnetic materials based on nearest neighbor exchange interaction between atomic spins. For artificially fabricated nanomagnets, it is those "small" magnetic energies, e.g. anisotropy, dipolar interaction and indirect exchange interaction that play crucial roles against the thermal fluctuation. We have developed strong capabilities to grow nanodot assemblies in ultrahigh vacuum with controllable size and density on/in both metallic and insulating templates. Based on our novel synthesis capability, we have studied artificial nanomagnets with tunable coupling strength via dimensionality control of the mediating electrons in one-dimensional (1-D), 2-D, and 3-D. We show that such kind of dimensional confinement provides a unique way to induce novel magnetic properties and to gain control of them. The research outlined in this work provides the science base to understand, modify, and manipulate the magnetic properties through dimensional confinement.

Keywords magnetic nanodots, surface states, indirect exchange, Curie temperature

PACS numbers 75.75.-c, 75.50.Bb, 73.20.-r

Contents

1 Introduction

Understanding the magnetic properties of nanometer scale dots is a central issue in magnetic materials [1–3]. Magnetic nanodots are not only important for applications such as high-density recording media, they are also of great interest for basic science research as a crossover from classical physics to quantum mechanics. To first order, assemblies of nano-scale magnetic dots are superparamagnetic [4]. In these systems, thermal energy, which causes fluctuation of the dots' magnetic moments, becomes significant enough to overcome the anisotropy energy barrier and randomize their orientation at the so-called blocking temperature. This typically occurs far below room temperature, giving rise to difficulties for applications in data storage devices.

If the spacing between magnetic nanodots is not too large, then usually the influence of magnetic interactions on the superparamagnetic behavior cannot be neglected [5, 6]. It is generally recognized that there exists two types of magnetic interactions: (i) the dipole–dipole magnetostatic interaction, and (ii) the electron mediated indirect exchange interaction. The importance of the dipolar interaction is most evident in high density recording media [7]. So far a large body of work has been devoted to studying the influence of the dipolar interaction on the barrier height for flipping the spin of each individual dot as well as the collective magnetic behavior of the dot assemblies [8–16]. In the strong interaction limit, Morup pointed out that a transition from a superparamagnetic state to an ordered state might occur

[17]. Indeed, this has been observed experimentally in a Cu(100) surface-supported Co island assembly, which exhibits a long range ferromagnetic order with a Curie temperature (T_c) of about 200 K when the Co islands approached the limit of two-dimensional (2-D) morphological percolation [18, 19]. The follow-up calculations confirmed the role of dipolar interaction in the observed ferromagnetic long-range order [20, 21].

The indirect exchange interaction, while showing significance in the spectacular oscillatory behavior of interlayer exchange coupling between two ferromagnetic layers separated by a nonmagnetic metal layer, has been much less discussed in terms of establishing long range ferromagnetic order in nanodot assemblies. This is not surprising because the oscillatory behavior, due to a spin dependent quantum size effect, should have little effect on promoting a global ferromagnetic order in a randomly distributed dot assembly. Strikingly, we have observed collective ferromagnetic behavior in two dimensional Fe dot assemblies on single crystal Cu(111) surface that originates from an indirect exchange interaction via the Cu(111) substrate [22]. These nanodots were grown using a novel method called buffer-layer assisted growth (BLAG) [23]. The ferromagnetic ordering temperature appears to be strongly dependent on the average spacing between the dots. For relatively dense nanodot assemblies, the exchange interaction is strong enough to allow the ferromagnetic order persist above room temperature. Recently, it was also shown theoretically that a strong ferromagnetic coupling between Fe nanodots on Cu(111) can be realized if the nanodots are partially embedded into the Cu substrate and a proper edge to edge distance between the magnetic nanostructures [24].

Besides the dipolar interaction and indirect exchange interaction, other nonclassical ferromagnetic interactions between nanodots include the magnetic Casimir force [25], preasymptotic coupling [26], and magnetic coupling by tunneling electrons [27, 28]. The former is generally a very weak force that arises from zero-point quantum fluctuation when the magnetic order changes. The middle is encountered on the surface of exchange-enhanced Pauli paramagnets like Pt and Pd, which are close to the onset of ferromagnetism (Stoner criterion). The latter, however, can be important if the tunneling barrier is small. In a specific case, the tunneling-induced coupling was reported to be the origin for the room temperature ferromagnetism in Fe dots on an insulating CaF2/Si(111) substrate [29]. Competing against thermal fluctuation, these magnetic interactions, along with the size-dependent magnetic anisotropy, should have strong influences on the overall magnetic behavior of a magnetic dot assembly, as schematically shown in Fig. 1. Using X-ray magnetic circular dichroism (XMCD), Fauth *et al.* have found single particle anisotropy of nanoparticles, substrate mediated magnetic coupling and dipolar interactions are all significantly contribute to the magnetic properties and response of the deposited Fe nanoclusters [30]. To understand the magnetism of a nanodot assembly, it becomes essential to distinguish the relative roles of magnetic anisotropy, dipolar interaction, indirect exchange interaction, and tunneling induced interaction. Although this is generally very challenging, some useful clues can be found:

1) Magnetic anisotropy is generally related to the properties such as crystallographic structure, size and shape of each individual particle, while the dot-dot interactions are strongly dependent on both the size and the spacing between the dots.

2) Dipolar interaction is much less affected by the electronic structure of the host matrix as compared to the indirect exchange interaction, while the tunneling interaction occurs only when the hosting template is an insulator.

3) Each interaction has its own characteristic dependence on the dot-dot spacing R. Dipolar interaction decays as $1/R^3$; indirect exchange interaction decays $1/R^D$ where D is the dimensionality of the mediating electrons, thus the coupling strength is strongly related with dimensionality confinement; and tunneling-induced coupling decays exponentially as e^{-R}.

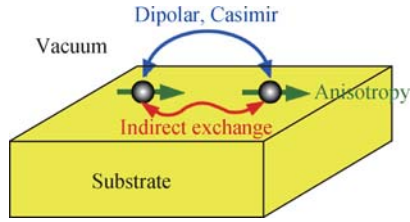

Fig. 1 Schematic demonstration of energy terms that can affect the magnetic behavior of a nanodot assembly.

Without a doubt, to apply these rules relies critically on the synthesis capabilities to control the size and spacing of magnetic dot assemblies in/on hosting templates of choice. Equally important is a set of powerful characterization tools for conducting a systematic investigation of the strength of magnetic anisotropy and the interactions as a function of dot–dot spacing, dot size and temperature.

The article is organized as follows, the second section is the technical details of the experiments; the magnetic coupling of Fe nanomagnets under 2-D, 3-D and 1-D confinement are discussed in the third, fourth and fifth section, respectively. The concluding summaries are listed at section six.

2 Buffer layer assisted growth

Direct deposition of Fe onto Cu(111) does not lead to dot formation [31]. The way to make the synthesis methodology general is to suppress or even eliminate the substrate

effect. An elegant approach, named buffer-layer assisted growth, as shown in Fig. 2, involves adsorbing inert gas elements (for example, 5N purity Xenon) on the Cu(111) substrate prior to the deposition of magnetic elements [22]. The Cu(111) substrate was prepared by cycles of 1 KeV Ne ion sputtering and annealing to 800 K, before it was cooled to about 30 K. The adsorption temperature is kept low enough to allow a solid phase of Xe to form on top of the substrate. The magnetic elements are subsequently deposited onto the inert buffer layer at low temperatures ($\sim$ 30 K). The low surface free energy and the high mobility of adatoms on Xe should allow nanodots to form easily on the buffer layer. The system is then gently warmed up to $\sim$ 300 K to sublimate the buffer layer, and the nanodots will softly land on the real substrate.

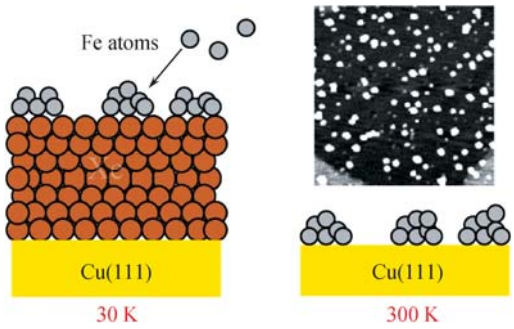

Fig. 2 Schematics of buffer layer assisted growth. The upper right is an STM image of 0.8 ML Fe dots on Cu(111). The Scanning area is 100 nm × 100 nm.

The BLAG is applicable to grow nanodots on many types of substrates. Moreover, it has a big advantage in terms of its easiness of tuning the average spacing and the size of the nanodots. This can be achieved by either changing the dosage of magnetic elements or the thickness of inert gas buffer layer. Near hemispherical clusters are found on Fe/Cu(111) [22], Fe/Pt(997) [26], Fe/Ag(111) and Fe/Cu(100) [32], while flat monolayer high islands are observed on Fe/Rh(111) and Co/Pt(111) due to complete wetting [32]. For the growth of Fe dots on Cu(111), the effects of independently varying the Fe dosage and the Xe exposure are displayed in Fig. 3. The density and the average size of the Fe dot assemblies are shown as a function of Fe dosage at a fixed Xe exposure of 200 L [1 langmuir (L) $=10^{-6}$ Torr·S] in (a), and as a function of Xe exposure at a fixed dosage of 1 ML (monolayer) Fe (nominal thickness) in (b). Apparently, changing the Xe exposure has a more pronounced affect on the dot size and density than varying the Fe dosage. The fact that the dot size increases with increasing Xe exposure can be understood to result from the enhanced likelihood for Fe clusters to collide and stick to each other as they work their way toward the Cu surface through a thicker buffer layer. Based on the information in Fig. 3, we can find Fe dosage / Xe exposure parameter combinations that produce two Fe dot assemblies with the same average dot size but different densities. In order to vary the dot densities continuously while fixing the average dot size, one has to expand Fig. 3 to a 3-D plot by obtaining the information of dot densities and size as a function of both Fe dosage and Xe exposure.

3 Origin of indirect exchange coupling and ferromagnetic order in Fe nanodot assemblies on Cu(111) surface

Fe/Cu(111) nanodots grown by the BLAG method are shaped like slightly flattened hemispheres with a rather random spatial distribution. Figure 4(a) shows the STM morphology of a typical Fe dot assembly formed by

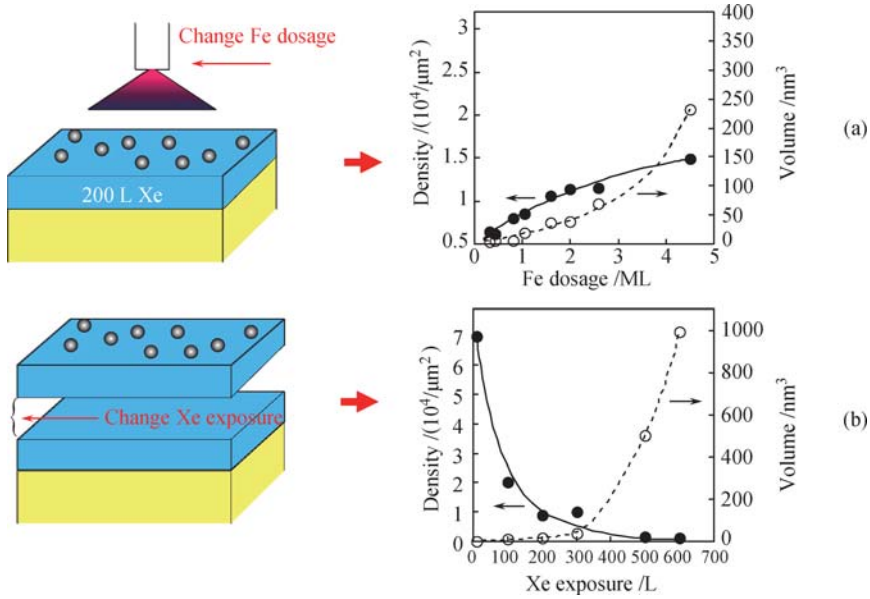

Fig. 3 Average size and density of Fe/Cu(111) dots assemblies as a function of Fe dosage **(a)**, and Xe exposure **(b)**. The solid and dashed lines are the guides for the eyes.

depositing the equivalent of 0.8 ML Fe assisted by 200 L Xe. The density of the nanodots, after a statistical analysis of images taken at various areas on the surface, is estimated to be about $8.05\times10^3/\mu m^2$. This yields an average dot volume of around 8.2 nm^3, i.e., $\sim$ 700 Fe atoms if assuming a *bcc* structure. Dot profile analysis indicates that the average height and the average width of the Fe dots are 1.4 nm and 3.5 nm, respectively. For such kind of dot size, the magnetic blocking temperature (without coupling) is estimated to be no more than 2 K if the bulk bcc Fe anisotropy (4.72×10^5 ergs/cm^3) is assumed. However, the in-plane longitudinal MOKE measurements of the Fe dot assembly shown in Fig. 4 (b) reveal clear ferromagnetic behavior as high as 90K. No perpendicular magnetization can be measured even at maximal field of 2400 Oe, indicating that the Fe dots have an in-plane easy magnetization axis.

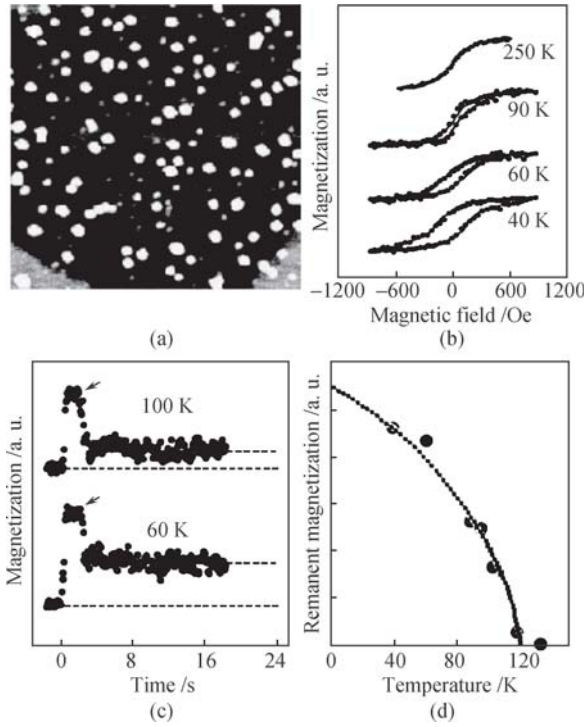

Fig. 4 **(a)** STM morphology (100 nm × 100 nm) of an Fe dot assembly on Cu(111) prepared with 0.8 ML Fe and 200 L Xe. **(b)** MOKE hysteresis loops of the Fe dot assembly at various temperatures. **(c)** Time dependence of the magnetization of the Fe dot assembly. An in-plane external field was applied at time "zero" and was switched off at the points in time indicated by the arrows. **(d)** Remanent magnetization of the Fe dot assembly as a function of temperature. The T_c is around 120 K.

The remanent magnetization (M_r) of the dot assembly, while strongly dependent on temperature, is remarkably stable with respect to time, as shown in Fig. 4(c). For the time-dependent magnetization measurements, the dot assembly was first demagnetized and then magnetized by an in-plane field of 2000 Oe. The external field was then removed at the point in time indicated by the arrows. The magnetization, after an initial rapid fall, remains very stable with respect to time even at elevated temperatures. Such stability allows us to define a meaningful critical temperature (T_c) above which M_r vanishes [$\sim$120 K as shown in Fig. 4(d)]. Note that the T_c value represents the dot–dot coupling strength rather than the magnetic moment of the nanodots, as indicated in Fig. 4(b) and (d). Based on the average dot size and density from STM experiments, the Monte Carlo simulation showed that the dipolar interaction does not lead to a T_c higher than 20 K even assuming an Ising-like anisotropy. Therefore, there must exist other factor(s) that is (are) responsible for the ferromagnetic stability.

Figure 5(a) shows T_c of Fe dot assemblies prepared on Cu(111), Cu(100), and Ge(111) surfaces as a function of Xe exposure. In all cases, the Fe nominal thickness is 1 ML. Evidently, under similar growth conditions, Fe dots consistently exhibit the highest T_c on Cu(111) and the lowest T_c on semiconducting Ge(111). This suggests that substrate mediated interaction dominates other factors including magnetic anisotropy (including shape anisotropy) and dipolar interaction in the Fe dot assemblies. Considering the fact that Cu(111) has much more pronounced surface states than Cu(100), Fig. 5(a) gives a strong indication that the substrate-mediated indirect coupling is likely associated with the presence of 2-D electron gas surfaces states. This argument is further backed experimental observations of T_c reduction after suppressing the surfaces states of Cu(111), which can be achieved by either capping a 8 ML Cu on the top of nanodot assemblies, or by roughening the Cu(111) surface using sputtering. As shown in Fig. 5(b), the Cu layer capping results in a reduction of T_c and thus the ferromagnetic coupling strength by a factor of 2. Figure 5(c) shows the T_c comparison of two similar Fe nanodot assemblies grown on smooth (with annealing) and rough (without annealing) Cu(111) surfaces. For the rough surface, the surface states are strongly disturbed and in turn lower the indirect coupling of the Fe nanodots. These crosschecks all indicate that the substrate-mediated indirect coupling is associated with the presence of 2-D electron gas surfaces states.

In general, electron mediated coupling between Fe nanodots belongs to the RKKY type of coupling, which shows oscillatory behavior and decays with distance and that can be fairly described as $\cos(2k_F R)/R^D$. Here R is the distance, and D is the dimensionality of the electrons. A most recent kinetic Monte Carlo simulations discusses the magnetic interaction of 2-D Fe nanostructures on Cu(111) surface [24]. The ferromagnetism can be stabilized if (i) Fe atoms are partially embedded into Cu(111) surface layer, and (ii) the edge to edge distance between the magnetic nanodots is below 1.5 nm and larger than 0.7 nm. As shown in the Fig. 6, the interaction energy between two embedded Fe clusters is nearly twice lower than that between two supported Fe clusters.

In real experiments, the embedded condition can be

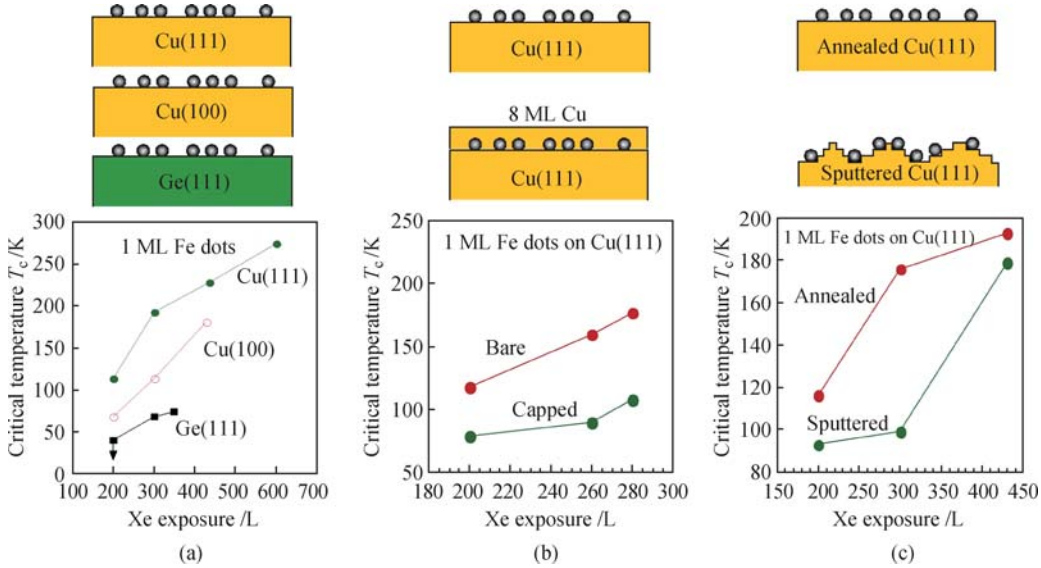

Fig. 5 **(a)** Critical temperature of Fe dot assemblies on various substrates of Cu(111), Cu(100), and Ge(111) as a function Xe exposure. The Fe nominal thickness is fixed at 1 ML in all cases. The arrow for the Fe/Ge(111) dots (200 L Xe) indicates that the T_c is below 40 K. **(b)** Critical temperature of 1 ML Fe dot assemblies on Cu(111) as a function of Xe exposure without and with 8 ML Cu capping, respectively. The capping of Cu on top of Fe dot assemblies significantly decreases the T_c. **(c)** The T_c of 1 ML Fe dot assemblies on a rough Cu(111) surface is also much lower that on an atomic flat surface.

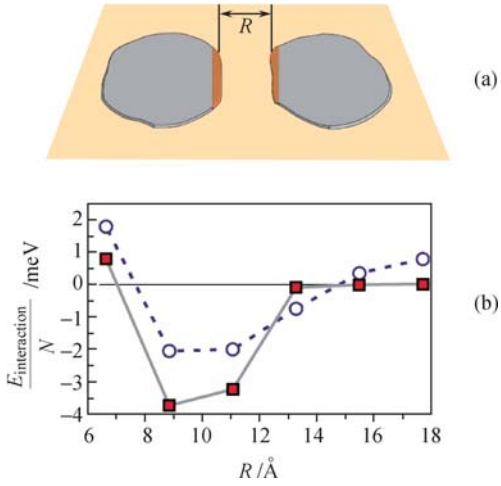

Fig. 6 **(a)** Two clusters on Cu(111) surface. Dark red stripes show the clusters edges governing the substrate mediated interaction between clusters. **(b)** The normalized substrate-mediated long range interaction between two supported Fe clusters (*circles, dashed lines*) ($N \gg 1$) and two embedded clusters (*squares, solid lines*) in ground-state magnetic configurations. Reproduced from Ref. [24].

realized if the sample is post annealed at room temperature because of Fe–Cu interface intermixing [33], which ensures sufficient spin polarization of the Cu(111) surface electronic states as the mediating electrons of the Fe nanodot assemblies. For the second condition, as indicated by Ignatiev *et al.* [24], we only need to consider the interaction between those neighboring nanodots whose edge-to-edge separation is less than 1.5 nm. Magnetic units without neighbors cannot participate in the magnetic ordering of an ensemble since exchange interaction between such clusters is small. By the statistic analysis, the nanodot assembly (428 L Xe, 1.05 ML Fe, 25 nm^3, $3\times10^3/\mu m^2$) in the upper left of Fig. 7, $\sim$ 30% of units have no neighbors, $\sim$ 50% have one neighbor, and $\sim$ 20% have larger number of neighbors, which gives a T_c of 150 K. To modify the dot-dot spacing, we further prepared a Fe nanodot assembly with same size but densities that differ by a factor of 5 (200 L Xe, 4.5 ML Fe, 25 nm^3, 1.5 $\times$ 10^4 μm^2). It is still far below the percolation threshold, as shown in the upper right of Fig. 7, $\sim$ 10% of units have no neighbors, $\sim$ 20% have one neighbor, and $\sim$ 70% have larger number of neighbors. The modification of nanodot spacing effectively increases the number of neighbors, and thus significantly enhances T_c to 325 K.

Because of the random spatial distribution of the Fe nanodots, the indirect exchange interaction should induce some degree of spin frustration in the dot assembly, especially, the spacing smaller than 0.7 nm would induce some kind of AFM coupling according to Ignatiev *et al.* [24] The degree of the spin frustration increases with increasing density and is reflected by the ratio of the remanent to saturation magnetization (M_r/M_s). Evidence of spin frustration in this system is shown in Fig. 7, as the M_r of the high-density dot assembly is less than a factor of 2 higher than that of the low-density assembly, despite the fact that its M_s value is 5 times higher. The power law fitting of the measured M_r vs. T data that is shown in Fig. 7 yields distinctly different critical exponents (β) for the two assemblies. In magnetic phase transition, a decreased critical exponent is often interpreted to result from a decrease in the dimensionality of a magnetic system [34]. The change that we observe, however, may not directly link to the critical behavior of a phase transition but due to the spin frustration.

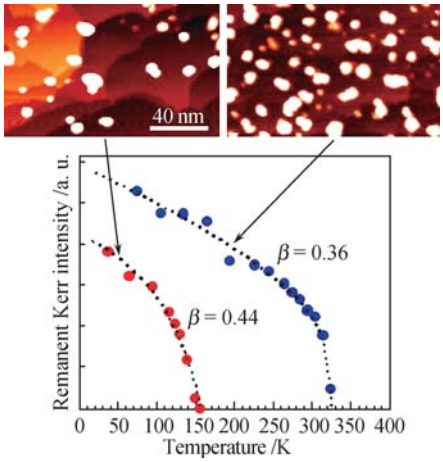

Fig. 7 *Top*: STM images of Fe/Cu(111) dots with equal average sizes ($\sim$ 25 nm^3) but different densities. *Bottom*: Their corresponding remanent magnetization measured as a function of temperature, with the critical exponent of power law fitting (*dashed lines*) indicated.

4 The three-dimensional indirect exchange coupling of Fe nanodots multilayers

The dimensionality of mediating electrons is vital for the coupling strength of Fe nanodots assemblies, because RKKY interaction decays with $1/R^D$, where D is the dimensionality. On Cu(111) surface, $D = 2$ if the coupling is through 2-D surface states. After capping of a 8 ML Cu layer or on a sputtered surface, the 2-D nature of the mediating electrons will be changed to 3-D-like and thus the coupling strength decays much faster with distance, which is evident in Fig. 5(b) and (c). To study the crossover behavior from 2-D to 3-D, we can stack these 2-D Fe nanodot assemblies with Cu spacer layers in between to form multilayer Fe nanodots, as illustrated in Fig. 8.

Based on our STM studies [35] (not shown here), in the growth process of the multilayer Fe nanodots, the morphology, including the average size and the density

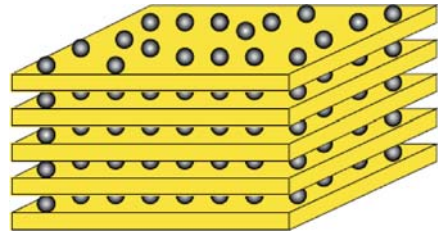

Fig. 8 Schematic view of multilayer dot assembly for magnetic critical behavior study.

of the Fe dots, varies little from layer to layer. The Fe dots have a slightly flattened hemisphere shape, with an average height of 1.2 nm, an average size of 3.2 nm, and a density of $1.2\times10^4\mu m^2$. When capped by a 12 ML thick Cu layer, the Fe dots are buried completely. Although the roughness of the Cu capping layers increases with increasing N, even at $N = 10$ the layer distribution of the exposed Cu surface is mostly limited within 3 layers. This implies that most of the Fe dots in each dot layer are distributed within three atomic layers along the direction normal to the film plane.

Figure 9(a) shows typical MOKE hysteresis loops measured from a Fe dot multilayer ($N = 4$) at various temperatures and (b) the ratio between M_r and M_s as a function of temperatures for three multilayer Fe dots ($N = 1$; 4; 10). The T_c, is about 80 K, 120 K, and 80 K for the $N = 1$; 4; 10 Fe dot multilayers, respectively. M_s increases linearly with increasing N in Fig. 9(c), which is expected since all the Fe dots contribute to the measured M_s under the saturation field. In contrast, T_c vs. N shows dramatically different behavior, which can be divided into three regions. With increasing N, T_c of the Fe dots initially increases from 80 K at $N = 1$ K to 120 K at $N = 4$ [region I in Fig. 9(d)]. When N is larger than 4, T_c starts to decrease, reaching a minimum temperature at $N = 7$ (region II). Remarkably, T_c at $N = 7$ is almost identical to T_c at $N = 1$, i.e., 80 K. Further increasing of N does not lead to any appreciable changes of the value of T_c (region III).

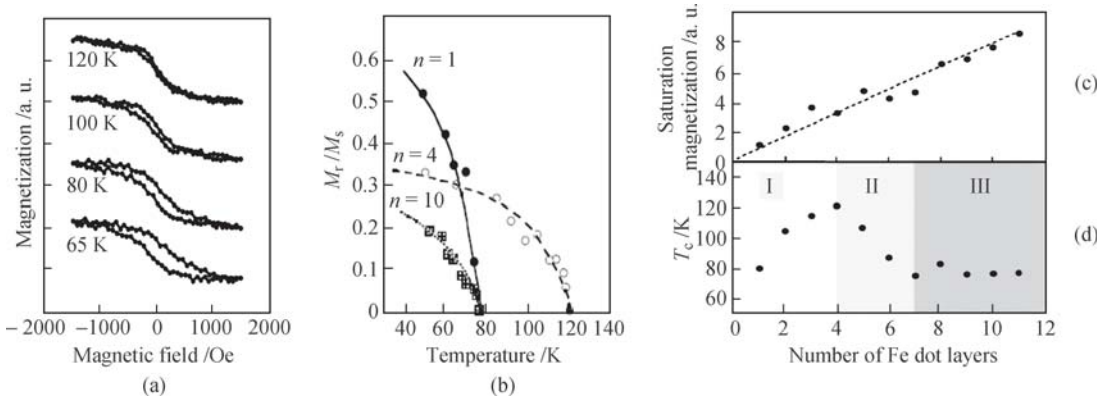

Fig. 9 **(a)** MOKE hysteresis loops of an $N = 4$ Fe dot multilayer at various temperatures. **(b)** M_r/M_s ratio as a function of temperature for $N = 1$, 4, and 10 Fe dot multilayers. **(c)** Saturation magnetization and **(d)** T_c as a function of the number of Fe dot layers N. With increasing N, the M_s increases linearly. T_c, however, changes nonmonotonically with increasing N, and regions I, II, and III are distinguished accordingly.

The results strongly suggest that the surface and bulk Fe dot layers have distinctly different magnetic behavior. For all thicknesses, the surface dot layer should be ferromagnetic, owing to the surface states of Cu(111) that mediates a ferromagnetic coupling. The situation becomes totally different for Fe dots in bulk layers, because the surface states no longer exist between the Fe dots. The Fe dots underneath the surface layer still interact with each other via magnetic dipolar interaction and/or RKKY interaction. Based on previous experimental studies of 3-D random distributed interacting magnetic nanoparticles [36–42], the Fe dots underneath the surface layer should have a spin-glass-like ground state, which is verified by the *ex situ* superconducting quantum interference device magnetometer measurement (SQUID). The thick Fe dot multilayer ($N = 11$) was capped by 20 ML of Cu before taking out of vacuum. The Cu capping should effectively destroy the Cu surface states in the topmost Fe dot layer. As shown in Fig. 10, the zero-field cooling and field cooling curves show strong deviation at low temperatures, which is consistent with a spin-glass like behavior. The corresponding spin glass temperature ($T_{\rm SG}$) is around 30 K and well below the $T_{\rm c}$ of the surface dot layer ($\sim$ 80 K).

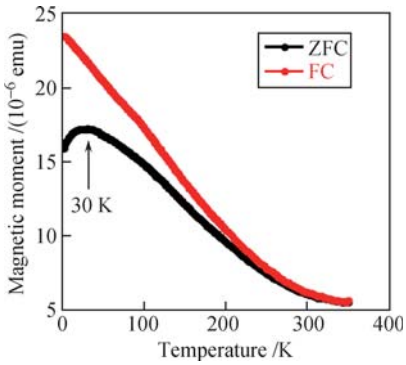

Fig. 10 Field cooling (FC) and zero-field cooling (ZFC) curves of a multilayer Fe dot ($N = 11$) measured at 50 Oe by SQUID magnetometer.

The surface ferromagnetism and bulk spin glass compete against each other, resulting in a change of magnetic structure with increasing thickness. The magnetic structure is schematically shown in Fig. 11. At low thickness (region I), the bulk Fe dot layers can still exhibit net magnetization due to the presence of surface ferromagnetic layer, which is why $T_{\rm c}$ increases with increasing N in this region. In region II, the influence of the surface becomes smaller, and the ferromagnetic alignment of the dot layer becomes weaker and, hence, $T_{\rm c}$ starts to decrease with increasing thickness. Eventually, the system moves into region III, where all Fe dot layers except the surface layer shows zero $M_{\rm r}$ above the corresponding critical temperature. The surface Fe dot layer in region III, however, remains ferromagnetic with same $T_{\rm c}$ as that of the Fe dot monolayer, because the strength of surface state mediated coupling should vary little with changing N.

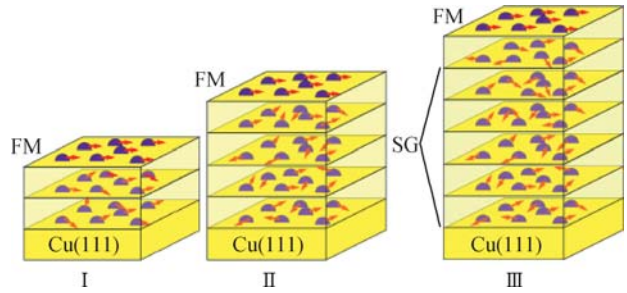

Fig. 11 Schematic picture of the speculated spin structures of the multilayer Fe nanodots in regions I, II, and III.

5 The one-dimensional indirect exchange coupling of Fe nanodots with lateral confinement

The Cu(111) surface state is characterized by a prominent Shockley-like 2-D electron gas, however, the dimensionality of the surface state can be modified if varying the terrace width d on vicinal surface [43]. For instance, the 2-D electron gas is confined by parallel step edge to form 1-D quantum well state when $d > 1.7$ nm [44, 45], and opens a gap at Fermi surface to form quasi-2-D super lattice state when $d \leqslant 1.7$ nm [46]. In previous section, we have shown that the indirect exchange coupling depends sensitively on the dimensionality of the mediating electrons when changing from 2-D to 3-D. In this section, we show that the lateral confinement of mediating electrons, i.e. from 2-D to 1-D, will offer another effective way to change dot-dot indirect coupling.

For consistency, we use a curved Cu(111) substrate with a gradient of vicinal angle from 0.8° to 7.2° (miscut towards $[\bar{1}\,\bar{1}\,2]$ with {100} type steps [43] as the substrate to grow Fe nanodots. Across the surface of such a curved substrate, the width of terraces varies continuously from a few hundred nanometer down to 1.7 nm. We find both the magnetic anisotropy and the ferromagnetic coupling of the Fe nanodot assemblies can be tuned by controlling the dimensionality of the Cu(111) surface states, but in different way [47].

Figure 12 shows typical hysteresis loops of a Fe nanodot assembly ($d \sim 3.1$ nm, $\rho \sim 1.4\times10^4/\mu{\rm m}^2$) measured from two surface locations with large (*red*) and small (*blue*) terrace width. The corresponding time-dependent remanent magnetization measured from both sites show a stable $M_{\rm r}$, which is similar to Fig. 4(c). The coupling strength of the Fe nanodots on the curved Cu(111) surface is found to depend strongly on the terrace width. Figure 13(a) shows the temperature dependent $M_{\rm r}/M_{\rm s}$ ratio of the 3.1 nm Fe nanodot assembly measured at surface locations with several representative terrace widths. Interestingly, the $T_{\rm c}$ for $w = 3.1$ nm appears to be higher than those measured from both wider (14.9 nm) and nar-

rower (1.7 nm) terraces. This non-monotonic behavior is most evident in Fig. 13(b), which shows the T_c values as a function of the terrace width. Two regimes can be identified with a sharp transition at $w = d$: in regime I, T_c increases with decreasing w, from 210 K at w =14.9 nm to 248 K at w =3.1 nm; and in regime II (1.7 nm $< w <$ 3.1 nm), the T_c falls rapidly.

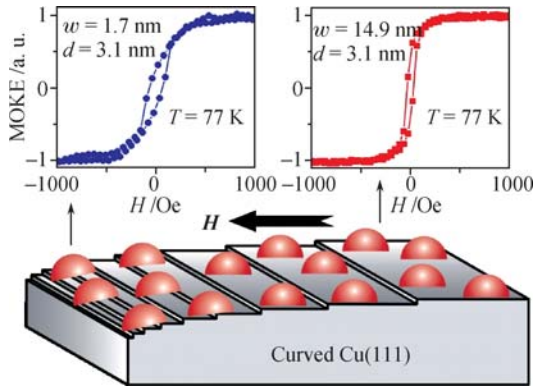

Fig. 12 Illustration of the Fe dot assembly on a curved Cu substrate. The inset is typical hysteresis loops of Fe dot assemblies atop high miscut angle (w = 1.7 nm, θ = 7.2°) and low miscut angle (w = 14.9 nm, θ = 0.8°) positions.

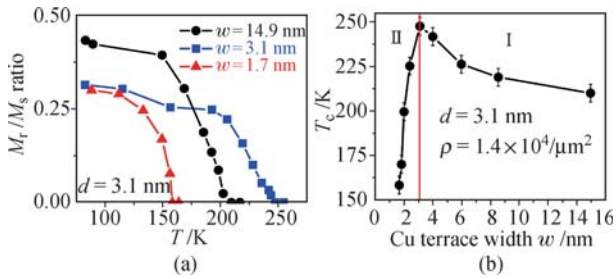

Fig. 13 **(a)** Temperature dependent M_r/M_s ratios of Fe dot assemblies with d = 3.1 nm measured on terrace widths of 14.9 nm, 3.1 nm and 1.7 nm. The w = 3.1 nm curve shows the highest T_c. **(b)** T_c as a function of w shows a maximum where $w = d$. In regime I, T_c increases with decreasing w, from 210 K on the 14.9 nm terrace to 248 K on the 3.1 nm terrace; and in regime II, the T_c falls rapidly between the 3.1 nm and the 1.7 nm terrace width.

The non-monotonic behavior of T_c does not likely originate from any structural factors of the Fe nanodots upon changing terrace width. Figure 14(a) shows a typical STM image of the morphological appearance of Fe nanodots on a stepped Cu(111) surface. Figure 14(b) shows statistical analysis of the dot size and density as a function of terrace width based on STM images. The morphological features of the Fe dots do not show appreciable changes with changing terrace width. As for the crystallographic structure, although we cannot determine whether the Fe dots are in fcc or bcc structure, we argue that in the buffer layer assisted growth, the Fe atoms first form clusters in the inert Xe buffer layer before they come in contact with the substrate. The relatively large size (∼1000 atoms) of the Fe nanodots means it is highly unlikely that the crystallographic structure will change with changing terrace width. Finally, the extent of Fe nanodots embedded in Cu does not likely change with terrace width. This is because the room temperature post annealing prior to magnetic measurements should allow the system to settle into an energetically favorable state. Although a direct proof that the Fe dots are indeed embedded in the copper surface layer is beyond the experimental resolution, Ignatiev *et al.* indicates that the Fe dots are likely already embedded in the Cu surface layer on large terraces [24]. The embedding process considered is limited to mainly the top surface layer, and is unlikely to change significantly with decreasing terrace width, because the Fe nanodots are rather large and thus "immobile". Moreover, even if the terrace width plays a role, the step edges will only assist the embedding process, and, according to Ignatiev *et al.*, we should observe an enhanced T_c with decreasing terrace width. This is in contradiction with the central experimental observation reported in the present paper. Therefore, we conclude that there is no significant variation of embedding process upon changing of terrace width.

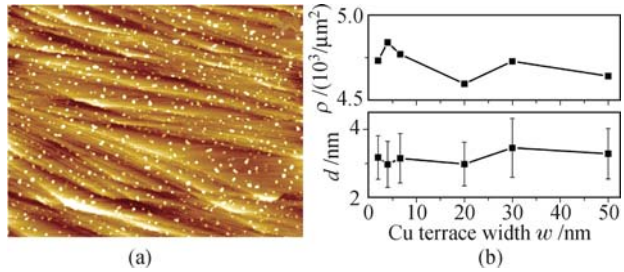

Fig. 14 **(a)** A typical STM image of Fe nanodots on Cu(111) substrate (500 nm × 392 nm). Even though the terrace width varies from 2 nm to 80 nm, no significant change of dot size and distribution is found. **(b)** The statistics of dot density and dot size distribution on various terrace width doesn't show any appreciable difference.

To understand the non-monotonic behavior of T_c with changing w, we further investigate the magnetic anisotropy of the Fe nanodot assemblies. Similar to those on a flat Cu(111) surface [22], the Fe nanodot assemblies on the curved surface also exhibit an in-plane easy magnetization since no magnetization signal can be detected by polar MOKE. Within the surface plane, however, the Fe nanodot assemblies on the curved surface show clear uniaxial anisotropy, in drastic contrast to the isotropic behavior of those on the flat surface. Figure 15(a) shows longitudinal MOKE hysteresis loops of the 3.1 nm Fe nanodot assembly. As summarized in the inset of Fig. 15(b), the M_r/M_s ratio measured along the step direction is significantly larger than that measured in the orthogonal direction independent of the terrace width. This indicates in-plane uniaxial anisotropy with easy axis along the step direction.

The saturation field (H_s) determined from the hard axis (in-plane but perpendicular to the step direction) magnetization loop can be used as a measure of the

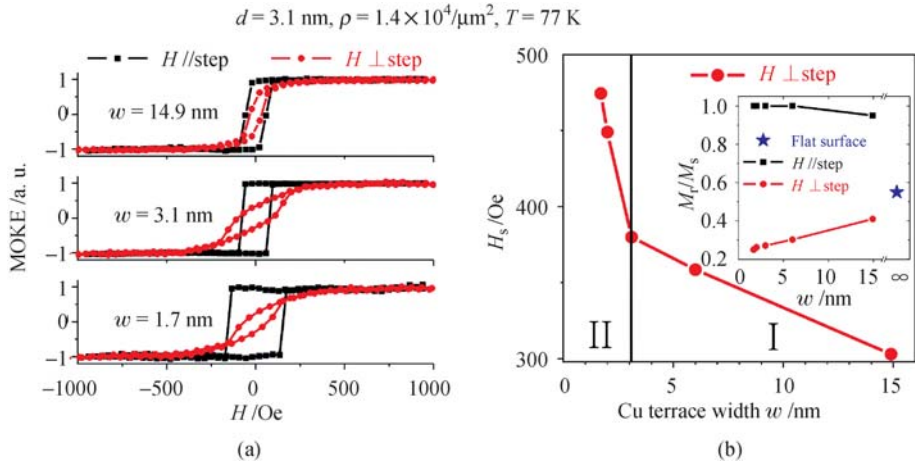

Fig. 15 **(a)** MOKE hysteresis loops of the Fe dot assemblies ($d = 3.1$ nm) on different terrace widths, $w = 14.9$ nm, 3.1 nm and 1.7 nm, respectively. Note that all show a clear uniaxial anisotropy with easy axis along the step. **(b)** Summarized saturation field H_s as a function of w indicates an enhancement of anisotropy. The inset is M_r/M_s ratio of hard and easy axis of vicinal surfaces with star indicating a flat surface.

uniaxial anisotropy strength. Figure 15(b) shows H_s of the 3.1 nm Fe nanodot assembly as a function of w. Again, two regimes can be distinguished. In regime I where $w > d$ (note that nanodots try to avoid contact with step edges unless they are forced to do so [22, 48]), H_s shows a clear trend of increasing with decreasing w. Therefore, the 1-D confinement results in an increase in the anisotropic strength, because the nanodots can "feel" the symmetry breaking through the surface states [49]. In regime II where $w < d$, H_s increases with a distinctly larger slope than in regime I. This rapid increase can be understood by the additional uniaxial anisotropy induced by the step edges. When $w < d$, each nanodot is forced to straddle across the step edges. The step edges further enhance the uniaxial anisotropy of each nanodot by the same mechanism that is commonly seen in magnetic thin films on vicinal surfaces [50, 51]. Because the number of steps underneath the nanodot increases with decreasing terrace width in regime II, it leads to a more rapid increase in the uniaxial anisotropy.

In low-dimensional magnetic systems such as ultrathin films [52, 53] and nanodots [54], in general, a larger anisotropy generally provides a larger energy barrier against thermal fluctuations and thus results in a higher T_c. In this regard, the increase of magnetic anisotropy should contribute to the increase of T_c in regime I of Fig. 13(b). However, if the anisotropy is the main cause, we should see an even more rapid increase of T_c with decreasing w in regime II, which contradicts the experimental results. Therefore the magnetic anisotropy alone cannot explain the non-monotonic behavior of T_c in the combined regime I + II.

Having ruled out any significant role of the magnetic anisotropy, we now consider how the dot–dot interaction can affect T_c and result in the nonmonotonic behavior. The changing terrace width should make substantial modification to the nature of the surface states which would likely lead to a significant change in the observed T_c. Let us consider the evolution of the surface states as a function of w. On large terraces ($w \geqslant d$), the surface states are confined by the terrace and form an array of 1-D quantum-well states. In this regime, the deposited nanodots try to avoid contact with the step edges. As w shrinks to $w < d$, the nanodots are forced to sit on top of step edges, as a result, effectively couple the surface states of neighboring terraces, causing a transition of the surface states from 1-D quantum well states to quasi-2-D. Hence the process of varying w clearly falls into two regimes. To demonstrate this point, we have calculated the density of states of (i) uncoupled 1-D quantum well states, and (ii) 1-D quantum well states with random links (coupling) between them. It is evident from Fig. 16 that even with 10% coverage, the system is already in the 2-D regime.

Once we realize the dramatic difference associated with the dimensionality change induced by the nanodots, we can focus on the two regimes separately. When the system is in the 1-D regime, the indirect exchange interaction decays as $1/R$ [55]. As w decreases further, the system enters the quasi-2-D regime, where the exchange interaction decays as $1/R^2$ for an isotropic Fermi surface [56]. Since the distance R between the nanodots is fixed, the sudden change in dimensionality of the surface states leads to the sharp drop in the T_c.

To calculate the RKKY interaction, one needs to know the energy spectra and wave functions of the electrons. One implication comes from the fact that the Fe nanodots are randomly located on the substrate, which requires the diagonalization of a rather complicated Hamiltonian. Since our focus is on the dimensionality change, we choose to consider a "clean" system where there is a periodic coupling between the surface electrons on neighboring terraces, as the RKKY range function is essentially unaffected by weak disorder [57–59]. The energy

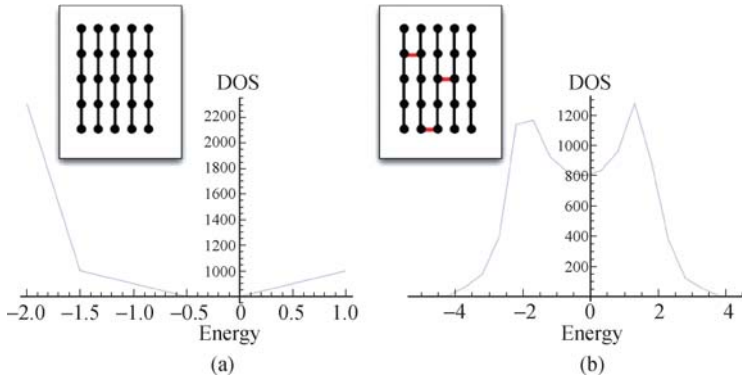

Fig. 16 **(a)** Density of states of uncoupled 1-D quantum well states. **(b)** Density of states of 1-D quantum well states coupled by the Fe nanodots (*red lines*).

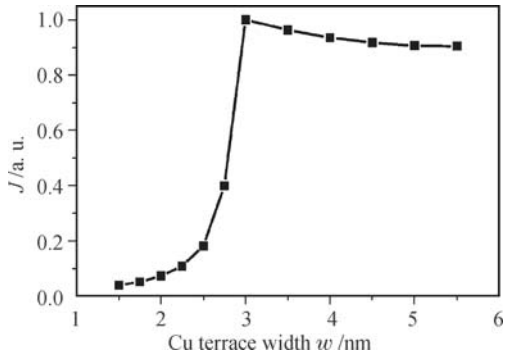

Fig. 17 Exchange interaction strength as a function of the terrace width obtained from a phenomenological model of surface-state mediated dot–dot coupling. The parameters used in the calculations correspond to the case where the Fe dot diameter $d = 3.1$ nm and density $\rho = 1.4 \times 10^4/\mu m^2$.

spectrum of the surface states thus takes the following form:

$$E_k = \frac{\hbar^2}{2m}\left[k_x^2 + \left(\frac{\pi}{w}\right)^2\right] - \lambda\cos(k_y w) \quad (1)$$

Here the x-axis is along the steps and the y-axis perpendicular to the steps. The first term comes from the fact that the electrons can freely move along the step direction and are confined by the steps in y-direction [60], and the second term represents the weak coupling of surface states on neighboring terraces, with λ measuring the coupling strength. $\lambda = 0$ for $w \geqslant d$ (corresponding to 1-D surface states) and increases with shrinking w when $w < d$. We consider the situation where w is small enough so that only the lowest sub-band is populated. In addition to the 1-D to 2-D transition, reducing w also raises the band bottom of the surface states thus gradually depopulating the surface states. Given the energy spectra in Eq. (1), the exchange interaction can then be calculated according to the standard RKKY theory [55, 56, 61–63]. The configuration-averaged exchange interaction $J_{\text{eff}} = \int \mathrm{d}\boldsymbol{r} J^{\text{RKKY}}(\boldsymbol{r})$ as a function of w is shown in Fig. 17, with $\lambda = 0.01\frac{\hbar^2}{w^2 m}\frac{d-w}{d}$. It is clear that the exchange interaction behaves differently in the two regimes. In regime I ($w \geqslant d$), the slight increase of the exchange interaction towards $w = d$ is due to the enhanced confinement with reduced w, originating from

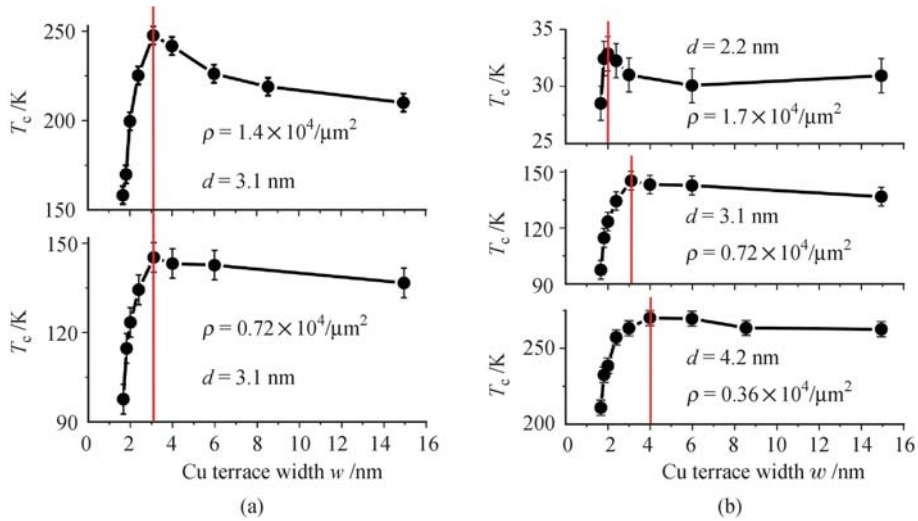

Fig. 18 **(a)** Density comparison of Fe dot assembles with dot size of 3.1 nm – note that both have maximum T_c at the same terrace width. **(b)** Terrace width dependence on T_c values for Fe dot assemblies of dot size of 2.2 nm, 3.1 nm, and 4.2 nm. The maximum T_c is always located at where $w = d$.

the characteristic form of the RKKY interaction in 1-D. The sharp drop in regime II ($w < d$) is due to the transition into the quasi-2-D case, where the interaction decays as $1/R^2$ instead of $1/R$. As w continues decreasing to $\sim \lambda_F/2$ (~ 1.5 nm), the surface states are completely depopulated, leading to a vanishing exchange interaction [64]. The closely matching trend of the exchange interaction from the model calculations and the observed T_c strongly suggest that the nanodot induced dimensionality change is the main mechanism responsible for the non-monotonic behavior of T_c.

If our argument holds, T_c should show a similar dependence on the terrace width for Fe nanodot assemblies having different size and density, i.e., reaching the maximum only when $w = d$. As shown in Fig. 18, this is indeed the case. We first compare two Fe nanodot assemblies of same size but different density in Fig. 18 (a). Apparently, both the T_c values peak at the same point. This occurs despite the fact that the T_c of the low-density nanodot assembly is considerably lower than that of the high-density one. Figure 18(b) again shows that the T_c of nanodot assemblies with different size all peak at the point where $w = d$. These crosschecks corroborate the overall physical interpretation reached from the phenomenological model. By tuning the size of Fe nanodot, we effectively bridge the electrons of neighbor terrace, the transition of Cu(111) vicinal surface from 1-D quantum well state to quasi-2-D supper lattice state is no longer limited at 7° [43], however, depends on the nanodot size.

6 Concluding summary

The indirect exchange coupling of Fe nanodots can be amplified due to the broken symmetry and the presence of surface states. As summarized schematically in Fig. 19, the artificial nanomagnets with tunable coupling strength via dimensionality control of the mediating electrons provide an effective way to induce novel magnetic properties and to gain control of them. The experimental results clearly demonstrate that the dot–dot indirect exchange coupling plays more significant role than other factors, including magnetic anisotropy and dipolar interaction. The research outlined in this work provides the science base to understand, modify, and manipulate the magnetic properties through dimensionality confinement. The effect of the modifications on the surface electronic structure are not limited to Cu(111). Substrates having pronounced surface states, like Ag(111), Au(111), and topological insulator, are all good templates. Our long-term goal is to develop the capability to design and fabricate the best dot/template combination that gives the most desired magnetic properties.

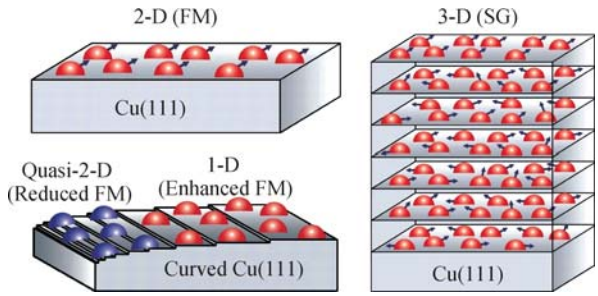

Fig. 19 Summarized dimensionality effects of mediating electrons to the indirect exchange coupling of Fe nanodot assemblies.

Acknowledgements We would like to thank valuable contributions of our collaborators from both experimental and theoretical sides. The experimental collaborators include J. P. Pierce, M. A. Torija, Z. Gai, A. P. Li, T. Z. Ward, and N. Widjaja. The theoretical effort mainly comes from D. Xiao, Z. Y. Zhang, T. C. Schulthess, and J. R. Shi. We would also like to thank E. W. Plummer, J. F. Wendelken and M. G. Stocks for insightful discussions.

References

1. 1. R. F. Wang, C. Nisoli, R. S. Freitas, J. Li, W. McConville, B. J. Cooley, M. S. Lund, N. Samarth, C. Leighton, V. H. Crespi, and P. Schiffer, Nature, 2006, 439: 303
2. S. Sun, C. B. Murray, D. Weller, L. Folks, and A. Moser, Science, 2000, 287: 1989
3. C. T. Black, C. B. Murray, R. L. Sandstrom, and S. Sun, Science, 2000, 290: 1131
4. H. Mamiya, I. Nakatani, and T. Furubayashi, Phys. Rev. Lett., 1999, 82(21): 4332
5. L. Wang, J. Ding, H. Z. Kong, Y. Li, and Y. P. Feng, Phys. Rev. B, 2001, 64(21): 214410
6. M. F. Hansen and S. Morup, J. Magn. Magn. Mater., 1998, 184(3): L262
7. D. J. Sellmyer, M. Yu, and R. D. Kirby, Nanostruct. Mater., 1999, 12(5–8): 1021
8. H. Zhang and M. Widom, Phys. Rev. B, 1995, 51(14): 8951
9. J.O. Andersson, C. Djurberg, T. Jonsson, P. Svedlindh, and P. Nordblad, Phys. Rev. B, 1997, 56(13): 983
10. D. Kechrakos and K. N. Trohidou, Phys. Rev. B, 1998, 58(18): 12169
11. T. Jonsson, P. Nordblad, and P. Svedlindh, Phys. Rev. B, 1998, 57(1): 497
12. R. W. Chantrell, N. Walmsley, J. Gore, and M. Maylin, Phys. Rev. B, 2000, 63: 024410
13. V. Russier, C. Petit, J. Legrand, and M. Pileni, Phys. Rev. B, 2000, 62(6): 3910
14. K. Yu. Guslienko, S. Choe, and S. Shin, Appl. Phys. Lett., 2000, 76(24): 3609
15. P. Politi and M. G. Pini, Phys. Rev. B, 2002, 66(21): 214414
16. V. Novosad, K. Guslienko, H. Shima, Y. Otani, S. Kim, K. Fukamichi, N. Kikuchi, O. Kitakami, and Y. Shimada, Phys. Rev. B, 2002, 65(6): 60402
17. S. Morup, Europhys. Lett., 1994, 28(9): 671
18. U. Bovensiepen, P. Poulopoulos, W. Platow, M. Farle, and K. Baberschke, J. Magn. Magn. Mater., 1999, 192: L386
19. P. Poulopoulos, P. Jensen, A. Ney, J. Lindner, and K.

Baberschke, Phys. Rev. B, 2002, 65(6): 064431
20. P. Politi1 and M. G. Pini, Phys. Rev. B, 2002, 66: 214414
21. P. J. Jensen and G. M. Pastor, Phys. Status Solidi (a), 2002, 189: 527
22. J. P. Pierce, M. A. Torija, Z. Gai, J. Shi, T. C. Schulthess, G. A. Farnan, J. F. Wendelken, E. W. Plummer, and J. Shen, Phys. Rev. Lett., 2004, 92(23): 237201
23. L. Huang, S. Chey, and J. Weaver, Phys. Rev. Lett., 1998, 80(18): 4095
24. P. A. Ignatiev, N. Negulyaev, A. Smirnov, L. Niebergall, A. Saletsky, and V. Stepanyuk, Phys. Rev. B, 2009, 80(16): 165408
25. G. Metalidis and P. Bruno, Phys. Rev. A, 2002, 66(6): 062102
26. R. Skomski, J. Zhang, V. Sessi, J. Honolka, A. Enders, and K. Kern, J. Appl. Phys., 2008, 103: 07D519
27. A. F. Bakuzis and P. C. Morais, Phys. Status Solidi (c), 2004, 1: 3332
28. V. N. Kondratyev and H. O. Lutz, Phys. Rev. Lett., 1998, 81(20): 4508
29. M. R. Scheinfein, K. E. Schmidt, K. R. Heim, and G. G. Hembree, Phys. Rev. Lett., 1996, 76(9): 1541
30. K. Fauth, G. E. Ballentine, C. Praetorius, A. Kleibert, N. Wilken, A. Voitkans, and K. H. Meiwes-Broer, Phys. Status Solidi (b), 2010, 247(5): 1170
31. J. Shen, M. Klaua, P. Ohresser, H. Jenniches, J. Barthel, C. Mohan, and J. Kirschner, Phys. Rev. B, 1997, 56(17): 11134
32. J. Honolka, V. Sessi, J. Zhang, S. Hertenberger, A. Enders, and K. Kern, Phys. Status Solidi (b), 2010, 247: 1063
33. H. L. Meyerheim, R. Popescu, D. Sander, J. Kirschner, O. Robach, and S. Ferrer, Phys. Rev. B, 2005, 71(3): 035409
34. F. Huang, M. Kief, G. Mankey, and R. Willis, Phys. Rev. B, 1994, 49(6): 3962
35. M. A. Torija, A. P. Li, X. C. Guan, E. W. Plummer, and J. Shen, Phys. Rev. Lett., 2005, 95(25): 257203
36. T. Jonsson, J. Mattsson, C. Djurberg, F. A. Khan, P. Nordblad, and P. Svedlindh, Phys. Rev. Lett., 1995, 75(22): 4138
37. C. Djurberg, P. Svedlindh, P. Nordblad, M. Hansen, F. Bødker, and S. Mørup, Phys. Rev. Lett., 1997, 79(25): 5154
38. T. Jonsson, P. Svedlindh, and M. F. Hansen, Phys. Rev. Lett., 1998, 81(18): 3976
39. H. Mamiya, I. Nakatani, and T. Furubayashi, Phys. Rev. Lett., 1998, 80(1): 177
40. H. Mamiya, I. Nakatani, and T. Furubayashi, Phys. Rev. Lett., 1999, 82(21): 4332
41. P. Jonsson, M. F. Hansen, and P. Nordblad, Phys. Rev. B, 2000, 61(2): 1261
42. Y. Sun, M. B. Salamon, K. Garnier, and R. S. Averback, Phys. Rev. Lett., 2003, 91(16): 167206
43. A. Mugarza, F. Schiller, J. Kuntze, J. Cordón, M. Ruiz-Osés, and J. E. Ortega, J. Phys.: Condens. Matter, 2006, 18(13): S27
44. M. F. Crommie, C. P. Lutz, and D. M. Eigler, Nature, 1993, 363: 524
45. F. Baumberger, M. Hengsberger, M. Muntwiler, M. Shi, J. Krempasky, L. Patthey, J. Osterwalder, and T. Greber, Phys. Rev. Lett., 2004, 92(19): 196805
46. F. Baumberger, M. Hengsberger, M. Muntwiler, M. Shi, J. Krempasky, L. Patthey, J. Osterwalder, and T. Greber, Phys. Rev. Lett., 2004, 92(1): 016803
47. L. Yin, D. Xiao, Z. Gai, T. Z. Ward, N. Widjaja, G. M. Stocks, Z. H. Cheng, E. W. Plummer, Z. Zhang, and J. Shen, Phys. Rev. Lett., 2010, 104(16): 167202
48. J. Zhang, D. Repetto, V. Sessi, J. Honolka, A. Enders, and K. Kern, Eur. Phys. J. D, 2007, 45(3): 515
49. L. Szunyogh, G. Zaránd, S. Gallego, M. C. Muñoz, and B. L. Györffy, Phys. Rev. Lett., 2006, 96(6): 067204
50. D. S. Chuang, C. Ballentine, and R. O'Handley, Phys. Rev. B, 1994, 49(21): 15084
51. Y. Z. Wu, C. Won, and Z. Qiu, Phys. Rev. B, 2002, 65(18): 184419
52. H. J. Choi, R. Kawakami, E. Escorcia-Aparicio, Z. Qiu, J. Pearson, J. Jiang, D. Li, and S. Bader, Phys. Rev. Lett., 1999, 82(9): 1947
53. R. Cheng, S. Bader, and F. Fradin, Phys. Rev. B, 2008, 77(2): 024404
54. L. Wang, J. Ding, H. Kong, Y. Li, and Y. Feng, Phys. Rev. B, 2001, 64(21): 214410
55. Y. Yafet, Phys. Rev. B, 1987, 36(7): 3948
56. B. Fischer and M. W. Klein, Phys. Rev. B, 1975, 11(5): 2025
57. A. Yu. Zuzin and B. Z. Spivak, JETP Lett., 1986, 43: 234
58. L. N. Bulaevskii and S. V. Panyukov, JETP Lett., 1986, 43: 240
59. A. Jagannathan, E. Abrahams, and M. J. Stephen, Phys. Rev. B, 1988, 37: 436
60. L. Bürgi, O. Jeandupeux, A. Hirstein, H. Brune, and K. Kern, Phys. Rev. Lett., 1998, 81(24): 5370
61. M. A. Ruderman and C. Kittel, Phys. Rev., 1954, 96: 99
62. T. Kasuya, Prog. Theor. Phys., 1956, 16: 45
63. K. Yosida, Phys. Rev., 1957, 106: 893
64. K. Morgenstern, K. F. Braun, and K. H. Rieder, Phys. Rev. Lett., 2002, 89(22): 226801